

Quantum Size Effects in the Terahertz Nonlinear Response of Metallic Armchair Graphene Nanoribbons

Yichao Wang and David R. Andersen

Abstract—We use time dependent perturbation theory to study quantum size effects on the terahertz nonlinear response of metallic graphene armchair nanoribbons of finite length under an applied electric field. Our work shows that quantization due to the finite length of the nanoribbon, the applied field distribution, and the broadening of the graphene spectrum all play a significant role in the resulting nonlinear conductances. In certain cases, these effects can significantly enhance the nonlinearity over that for infinitely-long metallic armchair graphene nanoribbon.

I. INTRODUCTION

GRAPHENE has many unique electronic, mechanical, thermal and optoelectronic properties [1]. A tunable Fermi level and linear dispersion relation near the Dirac point are some of the features that make graphene attractive for the study of nonlinear effects in the terahertz (THz) regime [2]–[7]. Various theoretical predictions of the generation of higher-order harmonics in graphene structures had been performed [8]–[13]. Recent experimental reports on the measurement of the THz nonlinear response in single- and multi-layer graphene [14]–[16] further demonstrate that graphene structures possess a strong nonlinear THz response. These theoretical and experimental studies demonstrate that, when compared to conventional parabolic semiconductor structures, unique graphene properties, such as linear energy dispersion, high electron Fermi velocity and tunable Fermi level, lead to a stronger nonlinear optical response in many 2D graphene structures [2]–[16].

Unlike the extensive research on the nonlinear response of 2D graphene structures, prior to our work, only the linear THz response [17], [18] and selection rules [19], [20] of graphene nanoribbons (GNR) for a linearly polarized electric field have been investigated. Thin GNRs (sub-20 nm) with smooth edges can be treated as quantum wires, not dominated by defects [21]. The reduced dimensionality of 2D graphene to a quasi 1D quantum wire for narrow GNR opens the study of new physics (including quantization of energy, momentum *etc.*). GNRs have two types of edges: armchair graphene nanoribbons (acGNR) and zigzag graphene nanoribbons (zzGNR). These two types of GNR shows distinct electronic characteristics due to the geometry and boundary conditions [22]–[25]. In

Yichao Wang is with the Department of Electrical and Computer Engineering, University of Iowa, Iowa City, IA, 52242 USA. (e-mail: yichao-wang@uiowa.edu).

David R. Andersen is with the Department of Electrical and Computer Engineering and the Department of Physics and Astronomy, University of Iowa, Iowa City, IA, 52242 USA. (e-mail: k0rx@uiowa.edu).

general, redistribution of the Dirac fermions induced by the applied electric field in momentum and energy space leads to large THz nonlinearities in GNR. The resulting nonequilibrium distribution predicts the conductivity components oscillating in time and space, and spatially homogeneous steady state components. As a result, nonlinear response in GNRs are sensitive to the applied field strength and polarization [7].

A widely used model, the perturbation of the Fourier expansion of the wave function first adopted by Wright *et.al.* [10] in the study of the THz nonlinear response of various 2D graphene systems [10]–[12], [26] has two important assumptions: *i*) the absence of coupling between the induced nonlinear response and the applied electric field distribution; and *ii*) charge carriers propagate with ideal ballistic transport in graphene, with the absence of broadening due to various scattering processes [27]. Velicky, Mašek and Kramer have developed a model of the AC ballistic/quasi-ballistic conductance in 1D quantum wires with an arbitrary spatial distribution of the applied electric field [28]–[30]. Wróbel *et.al.* measured and analyzed the role of reduced dimensionality in the quantized conductance of an GaAlAs/GaAs quantum wire [31], [32]. As thin GNRs with finite length in our study possess a low dimensional mesoscopic structure, it is natural to use these ideas to extend this analytical approach to the nonlinear response of thin GNRs with an applied electric field.

Carrier relaxation in graphene near the Dirac point is caused primarily by scattering of hot carriers [33]–[36]. Two typical carrier relaxation times have been reported, 25 ps for $E_F \ll 200$ meV, where 200 meV corresponds to the optical phonon energy [33] and a few ps for states involving optical phonon scattering [33]–[38]. Current limitations to the utilization of thin GNRs for nonlinear device applications result from scattering due to edge defects and hot carriers [34]–[36], [39]–[41]. Furthermore, edge disorder can affect the interband transition process due to the extra energy required to satisfy the conservation laws in the interband transition process [37], [42]. Our work focuses on the THz emission due to direct interband transition of graphene carriers with energy $\ll 200$ meV in thin metallic acGNR. Scattering due to hot carriers and optical phonons is reduced for the THz direct interband transition [35], [42], [43]. Further, scattering due to acoustic phonons is prohibited for these interband transition [43]. Therefore, carrier relaxation in finite GNR structures mainly depends on edge disorder and defects.

Theoretical studies show that non-perfect edges destroy the quantization of the conductance for GNRs [44]. However,

the rapid development of techniques for the synthesis of thin GNRs [21], [45], [46], show that thin GNR may have ultra smooth edges, higher mobility and longer carrier mean free path than expected theoretically. The recent reported synthesis of ultra thin acGNR (sub-10 nm) show that the electronic structure of ultrathin acGNR is not strongly affected by defects (kinks) [45], [46]. It is possible for thin GNR mesoscopic structures grown in the laboratory to show ballistic and quasi-ballistic transport. Scattering along the channel direction is greatly reduced in the ballistic and quasi-ballistic regime [47]. Such progress in the state of art of the growth of ultra thin GNR highlights the potential for quasi 1D GNR mesoscopic structures to be used in modern ultra-high-speed electronic and quantum devices [47]. Thus the study the nonlinear electrodynamics for thin metallic acGNR with an applied electric field with finite length in the mesoscopic regime is of particular significance today.

This paper is organized as follows: In Sec. II, we extend our analysis of thin metallic acGNR to the finite length case. We employ coupling due to the applied electric field distribution, and the intrinsic broadening of ideal graphene with the absence of edge defects to study the quantum effects due to finite size. In Sec. III, we apply our model to calculate the nonlinear THz conductance of thin metallic acGNR. We analyze the dependence of the third-order nonlinear terms on the ribbon length, temperature, and length of illumination. Following the introduction of broadening, we propose an effective critical length, characterizing the quantization of energy due to finite length impacting the continuum of states. Following this, we show that in metallic acGNR with length smaller than the effective critical length, the THz third-harmonic conductance is greatly enhanced to nearly the order of the THz third-order Kerr conductance in the THz window. This result shows that the tunability of thin metallic acGNR in the terahertz regime is increased. Finally, we present our conclusions in Section IV.

II. MODEL

Following the low energy model for GNR [22], [23], the unperturbed $\mathbf{k} \cdot \mathbf{p}$ Hamiltonian for states near the Dirac points may be written in terms of Pauli matrices as $H_{0,K} = \hbar v_F \boldsymbol{\sigma} \cdot \mathbf{k}$ for the \mathbf{K} valley and $H_{0,K'} = \hbar v_F \boldsymbol{\sigma} \cdot \mathbf{k}'$ for the \mathbf{K}' valley with \mathbf{k} (\mathbf{k}') the perturbation from the center of the \mathbf{K} (\mathbf{K}') valley. The time-independent (unperturbed) Hamiltonian for GNR may be written:

$$H_0 = \hbar v_F \begin{pmatrix} 0 & k_x - ik_y & 0 & 0 \\ k_x + ik_y & 0 & 0 & 0 \\ 0 & 0 & 0 & -k_x - ik_y \\ 0 & 0 & -k_x + ik_y & 0 \end{pmatrix} \quad (1)$$

with wave functions in the case of acGNR:

$$\psi_{n,s} = \frac{e^{ik_y y}}{2\sqrt{L_x L_y}} \begin{pmatrix} e^{-i\theta_{k_n, k_y}} e^{ik_n x} \\ se^{ik_n x} \\ -e^{-i\theta_{k_n, k_y}} e^{-ik_n x} \\ se^{-ik_n x} \end{pmatrix} \quad (2)$$

where L_x is the width of the acGNR in the \hat{x} direction,

L_y is the length of the acGNR in the \hat{y} direction, and $\theta_{k_n, k_y} = \tan^{-1}(k_n/k_y)$ is the direction of the isospin state. This Hamiltonian does not include intervalley scattering processes due to its block-diagonal character.

The width of acGNR is defined by $L_x = \frac{N}{2}a_0$. This determines the metallic or semiconductor character of the acGNR [22], [23]. In general, acGNR of $N = 3M - 1$ atoms wide along the zigzag edge, with M odd, are metallic, whereas all other cases are semiconducting. The energy dispersion relation arising from this model is doubly-degenerate, with one branch coming from each of the \mathbf{K} and \mathbf{K}' valleys.

Following our previous study of the THz third-order nonlinear conductance for thin metallic acGNR, an applied linearly-polarized electric field in the \hat{y} direction gives rise to the nonlinear conductance:

$$\begin{aligned} g_{y\nu}^{(i)}(\omega) &= \lim_{\Gamma \rightarrow 0} g_s g_v \sum_{m=-\infty}^{\infty} \sigma_{y\nu}^{(i)}(m, \omega) N(\epsilon) \\ &= \lim_{\Gamma \rightarrow 0} g_s g_v \frac{L_y}{2\pi} \int dk_y \sigma_{y\nu}^{(i)}(m, \omega) N(\epsilon) \end{aligned} \quad (3)$$

with $\nu = x, y$ the direction of the current and $\sigma_{y\nu}^{(i)}(m, \omega)$ the conductivity [27].

A. AC conductance

Due to the quasi-1D structure of the acGNR and the resultant quantization in k space, we need to consider the coupling of the applied electric field with the quantized k -states. The AC conductance $\tilde{g}(\omega)$ is defined in terms of the absorbed power $P(\omega)$ for an acGNR locally excited with electric field $\mathbf{E}(\mathbf{r}, \omega)$:

$$\tilde{g}(\omega) \equiv \frac{P(\omega)}{\phi^2(\omega)/2}, \quad \phi(\omega) = \int \mathbf{E}(\mathbf{r}, \omega) \cdot d\mathbf{r} \quad (4)$$

where $\phi(\omega)$ is the change of the electric potential in the irradiated region. The absorbed power may be expressed by the conductivity and the acting field as:

$$\tilde{g}(\omega) = \frac{1}{2} \int \frac{dk}{2\pi} \sigma(k, \omega) |E(k, \omega)|^2 \quad (5)$$

The i th order AC conductance for infinitely long acGNR $\tilde{g}_{y\nu}^{(i)}(\omega)$ is written [28]–[30]:

$$\tilde{g}_{y\nu}^{(i)}(\omega, L) = \frac{g_s g_v L_y}{2\pi} \int_{-\infty}^{+\infty} dk_y \sigma_{y\nu}^{(i)}(m, \omega) \left(\frac{\sin(k_y L/2)}{k_y L/2} \right)^2 \quad (6)$$

with L the length of illumination. For simplicity, we assume a constant field strength over the length of illumination L .

Defining $\omega_y = k_y v_F$, the corresponding angular frequency of k_y in GNR with a group velocity of v_F , we rewrite (6) for the third-order AC conductance as:

$$\tilde{g}_{y\nu}^{(3)}(\omega, L) = \sum_{l=1}^2 2 \int_0^\infty d\omega_y f_{y\nu}^{(\omega)}(\omega_y, \frac{\omega l}{2}) \delta(\omega_y - \frac{\omega l}{2}) \quad (7a)$$

$$\tilde{g}_{y\nu}^{(3)}(3\omega, L) = \sum_{l=1}^3 2 \int_0^\infty d\omega_y f_{y\nu}^{(3\omega)}(\omega_y, \frac{\omega l}{2}) \delta(\omega_y - \frac{\omega l}{2}) \quad (7b)$$

where $f_{y\nu}^{(\omega_0)}(\omega_y, \omega_0)$ is the coefficient associated with the corresponding $\delta(\omega_y - \omega_0)$ term in the expansion of the expression for conductance (see [27, eq. (37-38)]).

With an applied electric field \mathbf{E} linearly polarized along the longitudinal direction of an infinitely long acGNR (\hat{y} direction), for the metallic band where $k_{x,n} = 0$, the AC isotropic nonlinear conductance, with $\Gamma_\omega \rightarrow 0$ becomes [27]:

$$\tilde{g}_{yy}^{(1)}(\omega, L) = -g_0 \eta_x N\left(\frac{\omega}{2}\right) S\left(\frac{\omega}{2}, L\right) \quad (8a)$$

$$\tilde{g}_{yy}^{(3)}(\omega, L) = -g_0 \eta \eta_x \sum_{l=1}^2 \left(\frac{1}{2}\right)^{-z(l)} N\left(\frac{\omega l}{2}\right) S\left(\frac{\omega l}{2}, L\right) \quad (8b)$$

$$\tilde{g}_{yy}^{(3)}(3\omega, L) = -g_0 \eta \eta_x \sum_{l=1}^3 \left(-\frac{1}{2}\right)^{z(l)} N\left(\frac{\omega l}{2}\right) S\left(\frac{\omega l}{2}, L\right) \quad (8c)$$

similarly, the AC anisotropic nonlinear conductance is:

$$\tilde{g}_{yx}^{(1)}(\omega, L) = g_0 \eta_x N\left(\frac{\omega}{2}\right) S\left(\frac{\omega}{2}, L\right) \quad (9a)$$

$$\tilde{g}_{yx}^{(3)}(\omega, L) = g_0 \eta \eta_x N(\omega) S(\omega, L) \quad (9b)$$

$$\tilde{g}_{yx}^{(3)}(3\omega, L) = g_0 \eta \eta_x \sum_{l=1}^3 \left(-\frac{1}{2}\right)^{z(l)} N\left(\frac{\omega l}{2}\right) S\left(\frac{\omega l}{2}, L\right) \quad (9c)$$

with the thermal factor:

$$N(\omega) = \frac{\sinh\left(\frac{\hbar v_F |\omega|}{k_B T}\right)}{\cosh\left(\frac{\hbar f_\mu}{k_B T}\right) + \cosh\left(\frac{\hbar v_F |\omega|}{k_B T}\right)} \quad (10)$$

and the illumination factor:

$$S(\omega, L) = \text{sinc}^2\left(\frac{\omega L}{2v_F}\right) \quad (11)$$

where the quantum conductance $g_0 = e^2 / (4\hbar^2)$, Fermi level $E_F = \hbar f_\mu$, harmonic constant $z(l) = [1 - (-1)^l] / 2$, gain due to the width $\eta_x = (g_s g_v v_F) / (\omega L_x)$ and the coupling strength $\eta = (e^2 E_y^2 v_F^2) / (\hbar^2 \omega^4)$. The illumination factor $S(\omega, L)$ in (8) and (9) arises from the finite illumination length and is the square modulus of the Fourier transform of the applied field distribution. As a result of the inversion symmetry inherent in acGNR, the 2nd-order current makes no contribution to the total current.

The total third-order nonlinear conductance for metallic acGNR then can be expressed as:

$$\tilde{g}_{tot,y\nu}^{(3)}(\omega, L) = \tilde{g}_{y\nu}^{(3)}(\omega, L) e^{-i\omega t} + \tilde{g}_{y\nu}^{(3)}(3\omega, L) e^{-i3\omega t} + \text{c.c.} \quad (12)$$

This result shows that for metallic acGNR, the third-order nonlinear conductance is a superposition of two frequency terms: *i*) $\tilde{g}_{y\nu}^{(3)}(\omega, L)$, the third-order Kerr conductance term corresponding to the absorption of two photons and the simultaneous emission of one photon; and *ii*) $\tilde{g}_{y\nu}^{(3)}(3\omega, L)$, the third-order third-harmonic conductance term corresponding to the simultaneous absorption of three photons. The complex conjugate parts in (12) are for the emission process.

We observe that by taking the limit $L \rightarrow 0$, the ideal conductance and AC conductance in our definition are equivalent: $g_{\mu\nu}^{(i)}(\omega) = \tilde{g}_{\mu\nu}^{(i)}(\omega, 0)$. For $L = 0$, there is no coupling between the induced nonlinear response and the applied field distribution. Due to the current operator $qv_F \sigma_y \delta(\mathbf{r} - \mathbf{r}_{op})$ used in our previous work [27], we assume graphene carriers at \mathbf{r}_{op} interact only with the incoming photon field at \mathbf{r}_{op} . The conductance $g_{\mu\nu}^{(i)}(\omega)$ is a special case of the AC conductance $\tilde{g}_{\mu\nu}^{(i)}(\omega, L)$, and the AC conductance $\tilde{g}_{\mu\nu}^{(i)}(\omega, L)$ reduces to the ideal conductance $g_{\mu\nu}^{(i)}(\omega)$ at $L = 0$.

B. Broadening

We employ a Gaussian broadening model to study the impact on the nonlinear conductance due to spectral broadening of acGNR in the THz regime. This Gaussian broadening method has been widely used in the study of many graphene and GNR structures [48]–[50]. The Gaussian kernel,

$$Z_g(\omega_y, \omega) = \frac{1}{\sqrt{\pi} \Gamma_\omega} \exp\left[-\frac{(\omega_y - \omega)^2}{\Gamma_\omega^2}\right] \quad (13)$$

with $\Gamma_\omega = (2\tau \sqrt{\ln 2})^{-1}$ and τ the relaxation time, replaces the Dirac delta function in the integrand of (7).

In this work, we neglect edge defects in the acGNR. We further assume the broadening parameter remains a constant in the THz regime, and is invariant of the temperature and applied field strength E_y . We obtain the value $\tau = 25$ ps from [33, Table I] and therefore, the broadening parameter used in (13) becomes $\Gamma_\omega = 0.024$ THz. This choice of the broadening parameter is appropriate because the direct interband transition in the THz regime is well below the 200 meV optical phonon band. We note however, that our model can be extended to situations with larger carrier scattering. As τ is reduced, the quantization of the conductance tends to be dominated by other scattering processes. As a result, the mean free path of the carriers becomes shorter, and the interaction between adjacent states defined by the quantization condition becomes stronger.

C. Quantization due to finite length

In all real nanoribbons, the length L_y of the nanoribbon will be finite. This results in a discrete set of electronic states along the k_y direction, as opposed to the continuum of states that results for $L_y \rightarrow \infty$. In this case, the resulting third-order conductances are obtained by summing over the discrete set of states rather than integrating over the continuum.

In metallic acGNR, when $k_{x,n} = 0$, the energy dispersion relation may be written $\epsilon = s|m|\hbar\omega_{y0}$, with $\omega_{y0} = 2\pi v_F / L_y$. For a finite nanoribbon length of L_y and broadening Γ_ω , with $\omega_y = m\omega_{y0}$, the third-order AC conductance becomes:

$$\tilde{g}_{y\nu}^{(3)}(\omega, L, L_y, \Gamma_\omega) = \sum_{m=0}^{\infty} \sum_{l=1}^2 2f_{y\nu}^{(\omega)}(\omega_y, \frac{\omega l}{2}) Z_g(\omega_y, \frac{\omega l}{2}) \omega_{y0} \quad (14a)$$

$$\tilde{g}_{y\nu}^{(3)}(3\omega, L, L_y, \Gamma_\omega) = \sum_{m=0}^{\infty} \sum_{l=1}^3 2f_{y\nu}^{(3\omega)}(\omega_y, \frac{\omega l}{2}) Z_g(\omega_y, \frac{\omega l}{2}) \omega_{y0} \quad (14b)$$

III. RESULTS AND DISCUSSION

For our calculation, with an applied electric field $\mathbf{E} = \hat{y}E_y e^{-i\omega t}$, the corresponding magnetic vector potential is of the form $\mathbf{A} = \hat{y}\frac{E_y}{i\omega}e^{-i\omega t}$, which describes the absorption process in the interband transition. In what follows, we summarize the characteristics of the AC nonlinear conductance for all combinations of length of illumination and Fermi level, given in (14).

We consider acGNR with finite length L_y , for which there exists an energy quantization with quantum number m , for states of the linear bands near the Dirac points in metallic acGNR. To simplify the discussion, we present results for acGNR20, the armchair graphene nanoribbon $N = 20$ atoms wide, and the applied field strength is $E_y = 10\text{ kV/m}$ throughout the discussion.

We plot the isotropic and anisotropic AC conductances as a function of L_y with $T = 0\text{ K}$ and 300 K , and $L \rightarrow 0$ for intrinsic acGNR in Fig. 1. The frequency of the applied field is $f = 1\text{ THz}$. Due to the energy quantization resulting from finite L_y , interband transitions can only be excited for states coupled by the excitation frequency $2\pi f = \omega$, namely those where $\omega/2 = M\omega_{y0}/2$ (single-photon resonance), $\omega = M\omega_{y0}$ (two-photon resonance), and $3\omega/2 = 3M\omega_{y0}/2$ (three-photon resonance for the third-harmonic nonlinearity) where M is an integer and where $\omega_{y0} = 2\pi v_F/L_y$ is the separation between the discrete states. If M is odd, then $M/2$ and $3M/2$ are not integers and states at these energies do not exist. This implies that contributions from the $\omega/2$ and $3\omega/2$ components of the conductance are nearly zero (exactly zero in the absence of broadening). If M is even, $M/2$ and $3M/2$ are both integers, thus contributions from the $\omega/2$ and $3\omega/2$ components of the conductance are non-zero. In summary, for $M = fL_y/v_F$ even, (14) is equivalent to (8, 9). For M odd, the $N(\omega/2)$ and $N(3\omega/2)$ terms in (8, 9) are negligible. In Fig. 1, we can see clearly how the ribbon length L_y affects the conductance. For small L_y , the broadening is smaller than the separation between states and we observe quantization of the conductance. In essence, the acGNR behaves as a rectangular quantum dot. When L_y becomes longer, the states move closer together and there is overlap due to broadening for adjacent energy states. As a result, the overall conductance approaches a constant value. We arrive at an effective critical length $L_{yc}^{(\omega)} = 2v_F/3\Gamma_\omega$ bounding the quantum and continuum regions for the Kerr conductance. Similarly, the effective critical length for the third-harmonic conductance $L_{yc}^{(3\omega)} = v_F/\Gamma_\omega$. Both critical lengths are independent of f in the THz regime. For $\Gamma_\omega = 0.024\text{ THz}$, $L_{yc}^{(\omega)} \sim 28\text{ }\mu\text{m}$ and $L_{yc}^{(3\omega)} \sim 42\text{ }\mu\text{m}$. When L_y is greater than the effective critical length, the conductance converges to the conductance of an infinitely-long acGNR, and we enter the quasi-continuum regime due to the fact that the broadening now overlaps adjacent states. Such asymptotic behaviour can be observed in Fig. 1 when L_y is greater than the critical length.

In Fig. 2 we plot the temperature dependence of the isotropic and anisotropic AC conductances for several nanoribbon lengths L_y with $L \rightarrow 0$. The frequency of the applied field is $f = 1\text{ THz}$. For the Kerr conductances as shown in Figs.

2a and 2c: when $L_y = 7\text{ }\mu\text{m}$ ($M = 7$), the conductance is dominated by the $N(\omega)$ term; when $L_y = 16\text{ }\mu\text{m}$ ($M = 16$), both the $N(\omega/2)$ and $N(\omega)$ terms contribute; and when $L_y = 27\text{ }\mu\text{m}$, we arrive at the critical length and the conductance is nearly the same as that for the infinitely-long nanoribbon for $T \geq 0\text{ K}$. For the third-harmonic conductances as shown in Figs. 2b and 2d we observe similar behavior: when $L_y = 7\text{ }\mu\text{m}$ ($M = 7$), the conductance is dominated by the $N(\omega)$ term; when $L_y = 16\text{ }\mu\text{m}$ ($M = 16$), the $N(\omega/2)$, $N(\omega)$, and $N(3\omega/2)$ terms contribute; and when $L_y = 42\text{ }\mu\text{m}$, we arrive at the critical length and the conductance is nearly the same as that for the infinitely-long nanoribbon for $T \geq 5\text{ K}$.

In Fig. 3, we plot the isotropic nonlinear conductances as a function of the illumination length L . For the Kerr conductance plotted in Figs. 3a and 3b we note a series of antiresonances in the magnitude of the conductance. For the intrinsic nanoribbon, these antiresonances occur when the zeros of the illumination factor $S(\omega, L)$ are located at the same frequency as the states coupled by the excitation field of frequency f (those having non-negligible contributions from $N(\omega_y)$). For the Kerr conductance of the intrinsic nanoribbon with $L_y \rightarrow \infty$, both the $N(\omega/2)$ and $N(\omega)$ terms contribute to the conductance, resulting in an antiresonance spacing determined by setting the zeros in the illumination factor equal to $\omega/2$. This results in the set of antiresonances at $L = 2\text{ }\mu\text{m}, 4\text{ }\mu\text{m}, \dots$. For the extrinsic case, there are two mechanisms contributing to the antiresonances: 1) the zeros in the illumination factor, and 2) state blocking due to the Fermi level offset. For example, in Fig. 3a ($T = 0\text{ K}$), for the extrinsic nanoribbons transitions at $\omega/2$ are completely blocked, and therefore only the $N(\omega)$ term contributes, resulting in an antiresonance spacing determined by setting the zeros in the illumination factor equal to ω . This results in the set of antiresonances at $L = 1\text{ }\mu\text{m}, 2\text{ }\mu\text{m}, \dots$ for both M even and odd. In contrast, for Fig. 3b ($T = 300\text{ K}$), for the M odd case, the $N(\omega/2)$ contribution is negligible and we obtain a similar result as for the $T = 0\text{ K}$ case. However, for M even, the $N(\omega/2)$ term is not completely blocked, and as a result (setting the zeros in the illumination factor equal to $\omega/2$), we obtain antiresonances at $L = 2\text{ }\mu\text{m}, 4\text{ }\mu\text{m}, \dots$

For the third-harmonic conductance plotted in Figs. 3c and 3d, the behavior is even richer than for the Kerr conductance. While the set of primary antiresonances follows the discussion above, a pair of sidelobe resonances surrounding each primary resonance is also observed. These sidelobe resonances result from the fact that the $N(\omega/2)$ and $N(3\omega/2)$ terms in the expression for the conductance (8c) have the opposite sign of the $N(\omega)$ term. Thus, for certain non-zero values of the illumination factor $S(\omega, L)$, the positive and negative thermal factor contributions exactly cancel and the sidelobe antiresonances manifest themselves. Because the exact value of the thermal factor functions change with temperature, the locations of these sidelobe antiresonances also shift with temperature. This effect can also be observed in Figs. 1b and 1d.

We also note here that for $T = 0\text{ K}$, and $L_y \rightarrow \infty$, with a uniform illumination factor $S(\omega, L) = 1$ ($L \rightarrow 0$) the third-harmonic conductance is always zero for intrinsic nanoribbons and only non-zero over a limited frequency range

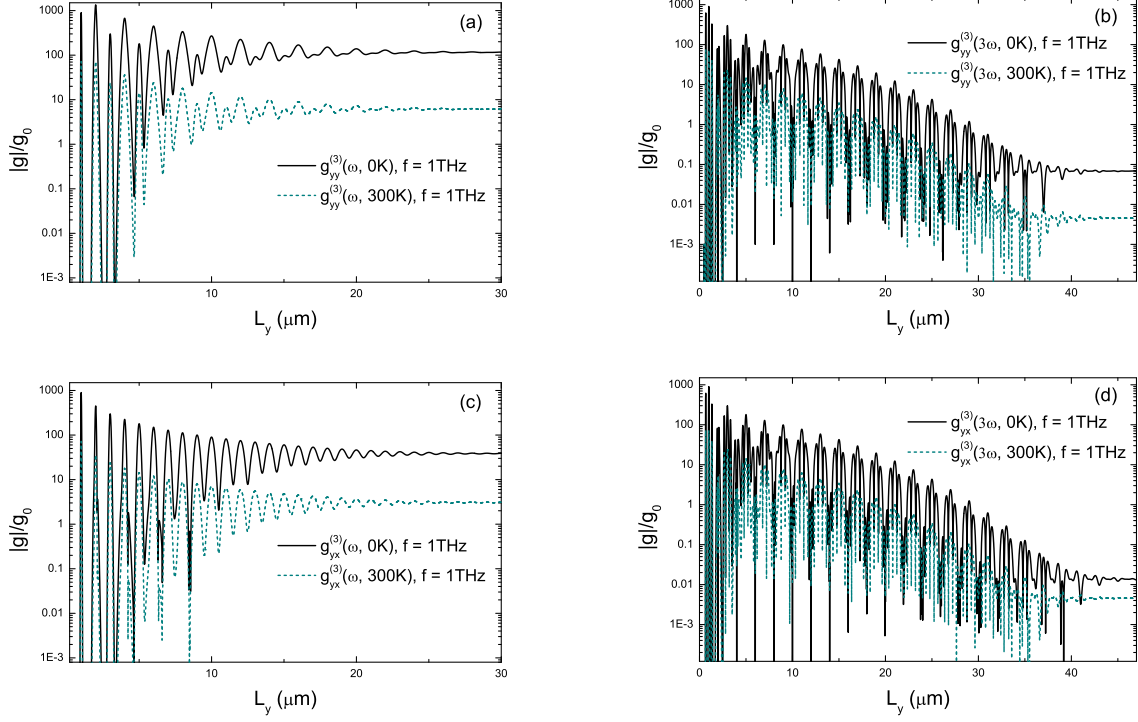


Fig. 1. Magnitude of the third-order nonlinear conductances in acGNR20 at $T = 0\text{ K}$ and 300 K as a function of nanoribbon length L_y . a) isotropic Kerr conductance, b) isotropic third-harmonic conductance, c) anisotropic Kerr conductance, and d) anisotropic third-harmonic conductance. For all plots, $f = 1\text{ THz}$, $E_F = 0$, $L = 0$, and $\Gamma_\omega = 0.024\text{ THz}$.

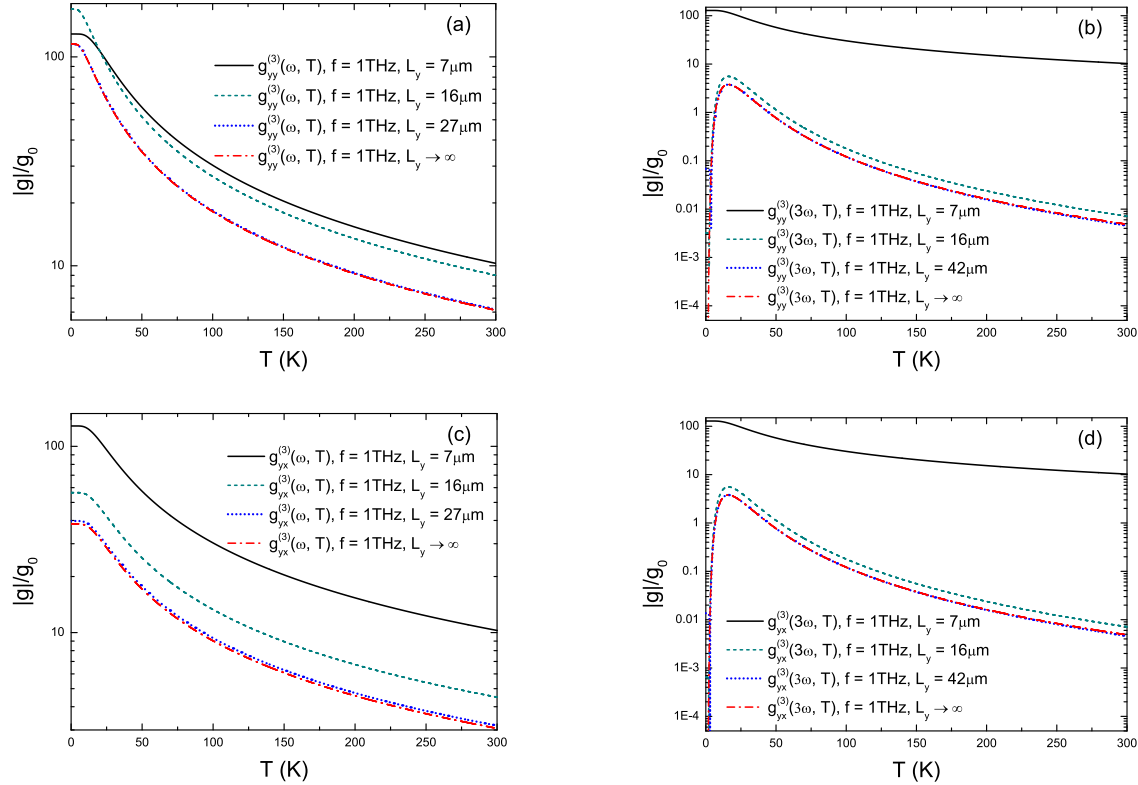


Fig. 2. Magnitude of the third-order nonlinear conductances in acGNR20 for various nanoribbon lengths as a function of temperature T . a) isotropic Kerr conductance, b) isotropic third-harmonic conductance, c) anisotropic Kerr conductance, and d) anisotropic third-harmonic conductance. For all plots, $f = 1\text{ THz}$, $E_F = 0$, $L = 0$, and $\Gamma_\omega = 0.024\text{ THz}$.

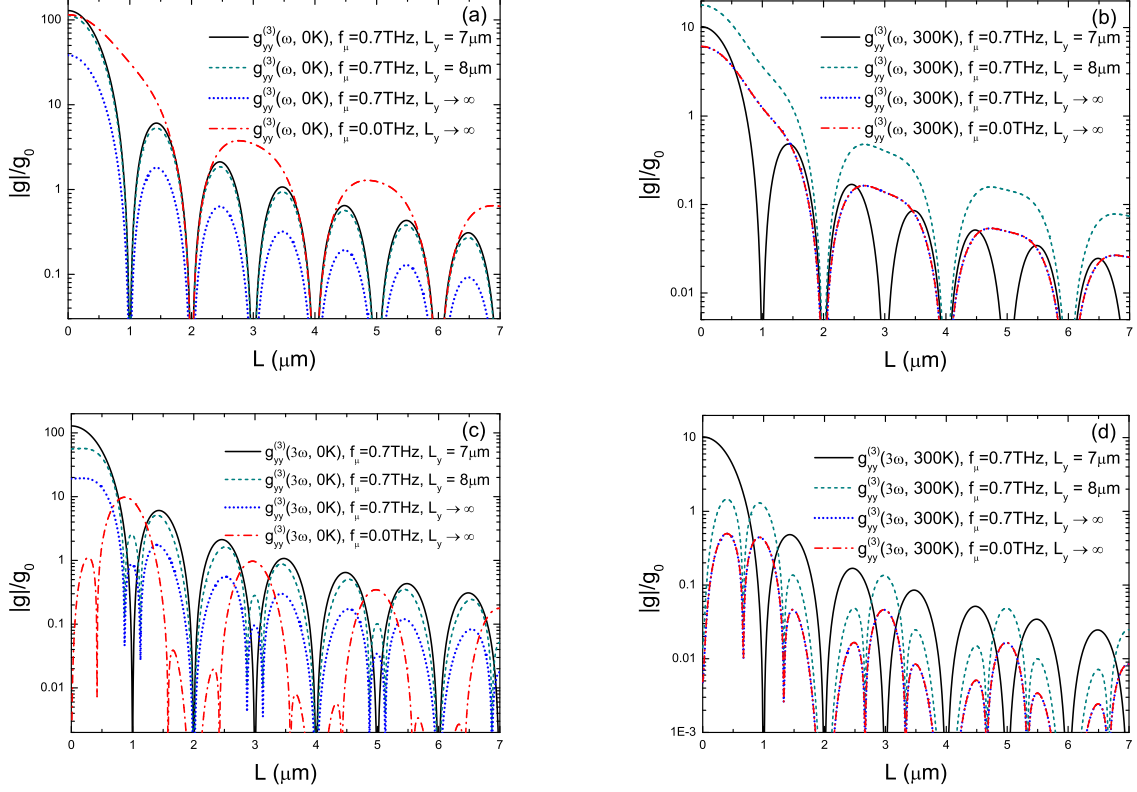


Fig. 3. Magnitude of the third-order nonlinear conductances in acGNR20 for various nanoribbon lengths and Fermi levels as a function of illumination length L . a) isotropic Kerr conductance, b) isotropic third-harmonic conductance, c) anisotropic Kerr conductance, and d) anisotropic third-harmonic conductance. For all plots, $f = 1$ THz.

for extrinsic nanoribbons ($2|f_\mu|/3 \leq f \leq 2|f_\mu|$) [27]. By extending the illumination range L (and therefore modulating the illumination factor) it is possible to enhance the third-harmonic conductance in these conditions so that for particular illumination lengths L , the third-harmonic conductance becomes of the order of the Kerr conductance magnitude.

In the interest of brevity, we do not plot the anisotropic nonlinear conductances, but simply note that the expression for the Kerr conductance contains only an $N(\omega)$ term. As a result, the characteristics of the anisotropic Kerr conductance follows closely that of the isotropic Kerr conductance with resonances at $L = 1 \mu\text{m}, 2 \mu\text{m}, \dots$ as discussed above. On the other hand, the anisotropic third-harmonic conductance contains all of the richness of its isotropic counterpart.

Fig. 4 illustrates the overall impact of the various quantum size effects we have discussed above on the magnitude of the third-order Kerr and third-harmonic conductances. In Figs. 4a and 4b, we plot the isotropic Kerr and third-harmonic conductances for several values of nanoribbon length L_y , illumination length L , temperature, and excitation frequency. The oscillatory nature of these curves highlights the interplay between the thermal factor (and thermal factor cancellation in the case of the third-harmonic conductance), state blocking, and the illumination factor. While the overall envelope of the conductances decay with increasing frequency as expected (generally following the results for the $L_y \rightarrow \infty, L \rightarrow 0$ case), there is clearly a richness in the detailed behavior governed

by the exact characteristics of the illumination and sample geometries. Similar effects are noted in Figs. 4c and 4d for the anisotropic nonlinear conductances as well. It is also useful to point out here that it should be possible to modify this dynamical behavior by apodizing [51] the applied THz electric field. For example, by using a Gaussian-apodized profile for the applied electric field, it should be possible to eliminate the antiresonances induced by the illumination factor $S(\omega, L)$. This would significantly reduce the oscillatory character of the results presented in Fig. 4.

IV. CONCLUSION

In this paper, we report detailed calculations of the quantum size effects on the nonlinear third-order conductances of acGNR. We show that effects due to both the size of the nanoribbon, as well as the size and spatial profile of the excitation field are important in determining the nonlinear response of acGNR. We model the third-order THz response of finite thin metallic acGNR using a semi-analytical approach. We employ Fourier analysis to solve the nonlinear Dirac equation using time-dependent perturbation theory. We show that both intrinsic and extrinsic metallic acGNR with finite length exhibit strong nonlinear effects, and quantization effects due to finite length from the THz to the FIR regime under an applied electric field with amplitude less than 10 kV/m.

We note that recently, ultrathin acGNR with widths $L_x < 10 \text{ nm}$ have been successfully synthesized [45], [46]. These

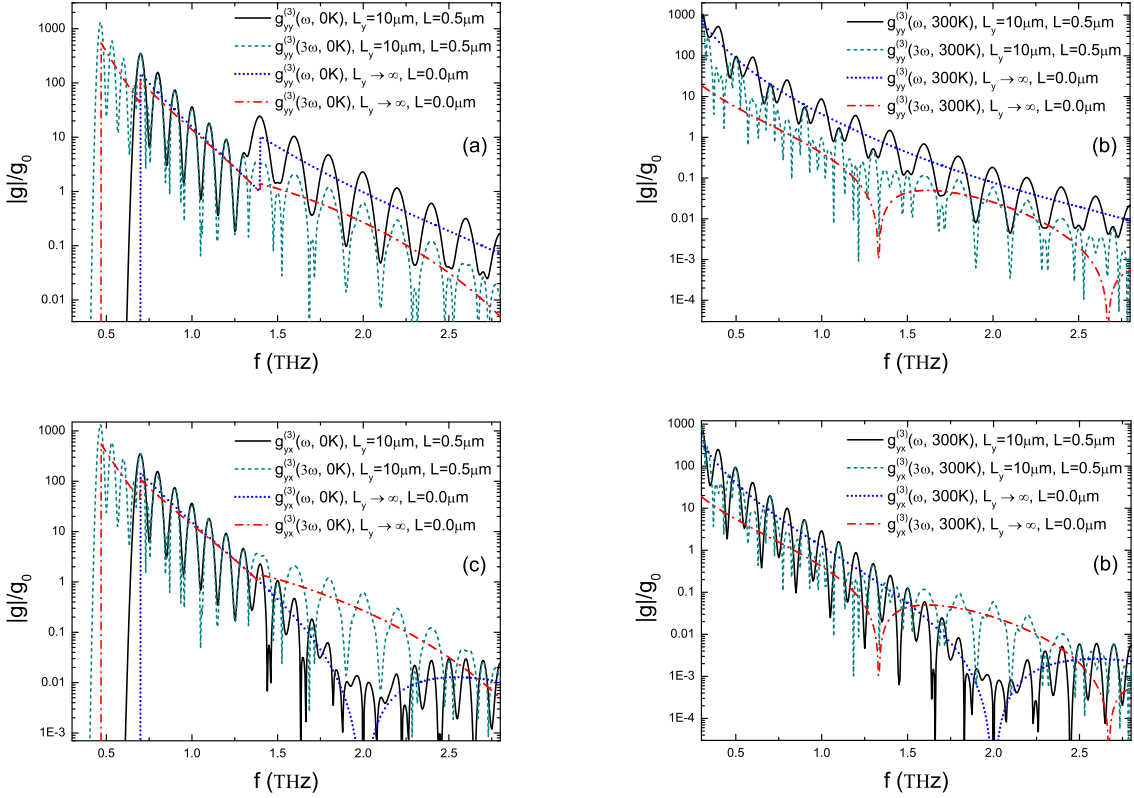


Fig. 4. Magnitude of the third-order nonlinear conductances in acGNR20 for various nanoribbon and illumination lengths, and temperatures as a function of excitation frequency f . a) isotropic Kerr and third-harmonic conductances at $T = 0$ K, b) isotropic Kerr and third-harmonic conductances at $T = 300$ K, c) anisotropic Kerr and third-harmonic conductances at $T = 0$ K, and d) anisotropic Kerr and third-harmonic conductances at $T = 300$ K. For all plots, $E_F/h = 0.7$ THz.

results, coupled with the results presented here, suggest that experimental measurement of the THz nonlinear response in thin metallic acGNR in the ballistic and quasi-ballistic regimes should be possible at relatively low excitation field strengths. The small critical field strength at room temperature implies that thin metallic acGNR have significant potential for nonlinear device applications. Notably, the enhancement of the third-order third-harmonic nonlinearity with small changes in Fermi level and finite length at room temperature indicates that metallic acGNR may provide the basis for developing a sensitive graphene-based detector, broadband modulator or oscillator over a wide range of temperatures.

REFERENCES

- [1] D. Abergel, V. Apalkov, J. Berashevich, K. Ziegler, and T. Chakraborty, "Properties of graphene: a theoretical perspective," *Advances in Physics*, vol. 59, no. 4, pp. 261–482, 2010.
- [2] S. Mikhailov, "Non-linear electromagnetic response of graphene," *EPL (Europhysics Letters)*, vol. 79, no. 2, p. 27002, 2007.
- [3] A. C. Neto, F. Guinea, N. Peres, K. S. Novoselov, and A. K. Geim, "The electronic properties of graphene," *Reviews of Modern Physics*, vol. 81, no. 1, p. 109, 2009.
- [4] E. Hendry, P. J. Hale, J. Moger, A. K. Savchenko, and S. A. Mikhailov, "Coherent nonlinear optical response of graphene," *Physical Review Letters*, vol. 105, no. 9, p. 097401, 2010.
- [5] S. D. Sarma, S. Adam, E. Hwang, and E. Rossi, "Electronic transport in two-dimensional graphene," *Reviews of Modern Physics*, vol. 83, no. 2, p. 407, 2011.
- [6] T. Gu, N. Petrone, J. F. McMillan, A. van der Zande, M. Yu, G.-Q. Lo, D.-L. Kwong, J. Hone, and C. W. Wong, "Regenerative oscillation and four-wave mixing in graphene optoelectronics," *Nature Photonics*, vol. 6, no. 8, pp. 554–559, 2012.
- [7] M. Glazov and S. Ganichev, "High frequency electric field induced nonlinear effects in graphene," *Physics Reports*, vol. 535, no. 3, pp. 101–138, 2014.
- [8] S. Mikhailov and K. Ziegler, "Nonlinear electromagnetic response of graphene: frequency multiplication and the self-consistent-field effects," *Journal of Physics: Condensed Matter*, vol. 20, no. 38, p. 384204, 2008.
- [9] S. Mikhailov, "Theory of the nonlinear optical frequency mixing effect in graphene," *Physica E: Low-Dimensional Systems and Nanostructures*, vol. 44, no. 6, pp. 924–927, 2012.
- [10] A. Wright, X. Xu, J. Cao, and C. Zhang, "Strong nonlinear optical response of graphene in the terahertz regime," *Applied Physics Letters*, vol. 95, no. 7, p. 072101, 2009.
- [11] Y. S. Ang, S. Sultan, and C. Zhang, "Nonlinear optical spectrum of bilayer graphene in the terahertz regime," *Applied Physics Letters*, vol. 97, no. 24, p. 243110, 2010.
- [12] Y. S. Ang and C. Zhang, "Subgap optical conductivity in semihydrogenated graphene," *Applied Physics Letters*, vol. 98, no. 4, p. 042107, 2011.
- [13] M. Gullans, D. E. Chang, F. H. L. Koppens, F. J. Garcia deAbajo, and M. D. Lukin, "Single-photon nonlinear optics with graphene plasmons," *Physical Review Letters*, vol. 111, no. 24, p. 247401, 2013.
- [14] I. Maeng, S. Lim, S. J. Chae, Y. H. Lee, H. Choi, and J.-H. Son, "Gate-controlled nonlinear conductivity of dirac fermion in graphene field-effect transistors measured by terahertz time-domain spectroscopy," *Nano Letters*, vol. 12, no. 2, pp. 551–555, 2012.
- [15] N. Kumar, J. Kumar, C. Gerstenkorn, R. Wang, H.-Y. Chiu, A. L. Smirl, and H. Zhao, "Third harmonic generation in graphene and few-layer graphite films," *Physical Review B*, vol. 87, no. 12, p. 121406, 2013.
- [16] H. A. Hafez, I. Al-Naib, M. M. Dignam, Y. Sekine, K. Oguri, F. Blanchard, D. G. Cooke, S. Tanaka, F. Komori, H. Hibino *et al.*, "Nonlinear

terahertz field-induced carrier dynamics in photoexcited epitaxial monolayer graphene,” *Physical Review B*, vol. 91, no. 3, p. 035422, 2015.

[17] Z. Duan, W. Liao, and G. Zhou, “Infrared optical response of metallic graphene nanoribbons,” *Advances in Condensed Matter Physics*, vol. 2010, 2010.

[18] W. Liao, G. Zhou, and F. Xi, “Optical properties for armchair-edge graphene nanoribbons,” *Journal of Applied Physics*, vol. 104, no. 12, p. 126105, 2008.

[19] K. I. Sasaki, K. Kato, Y. Tokura, K. Oguri, and T. Sogawa, “Theory of optical transitions in graphene nanoribbons,” *Physical Review B*, vol. 84, no. 8, p. 085458, 2011.

[20] H. Chung, M. Lee, C. Chang, and M. Lin, “Exploration of edge-dependent optical selection rules for graphene nanoribbons,” *Optics Express*, vol. 19, no. 23, pp. 23 350–23 363, 2011.

[21] X. Wang, Y. Ouyang, L. Jiao, H. Wang, L. Xie, J. Wu, J. Guo, and H. Dai, “Graphene nanoribbons with smooth edges behave as quantum wires,” *Nature nanotechnology*, vol. 6, no. 9, pp. 563–567, 2011.

[22] L. Brey and H. A. Fertig, “Electronic states of graphene nanoribbons studied with the dirac equation,” *Physical Review B*, vol. 73, no. 23, p. 235411, 2006.

[23] L. Brey and H. Fertig, “Elementary electronic excitations in graphene nanoribbons,” *Physical Review B*, vol. 75, no. 12, p. 125434, 2007.

[24] D. R. Andersen and H. Raza, “Plasmon dispersion in semimetallic armchair graphene nanoribbons,” *Phys. Rev. B*, vol. 85, p. 075425, 2012.

[25] D. R. Andersen and H. Raza, “Collective modes of massive dirac fermions in armchair graphene nanoribbons,” *Journal of Physics: Condensed Matter*, vol. 25, no. 4, p. 045303, 2013.

[26] Y. S. Ang, Q. Chen, and C. Zhang, “Nonlinear optical response of graphene in terahertz and near-infrared frequency regime,” *Frontiers of Optoelectronics*, vol. 8, no. 1, pp. 3–26, 2015.

[27] Y. Wang and D. R. Andersen, “First-principles study of the terahertz third-order nonlinear response of metallic armchair graphene nanoribbons,” *arXiv preprint arXiv:1603.06027*, 2016.

[28] J. Mašek and B. Kramer, “On the conductance of finite systems in the ballistic regime: dependence on fermi energy, magnetic field, frequency, and disorder,” *Zeitschrift für Physik B Condensed Matter*, vol. 75, no. 1, pp. 37–45, 1989.

[29] B. Velicky, J. Mašek, and B. Kramer, “ac-conductance of an infinite ideal quantum wire in an electric field with arbitrary spatial distribution,” *Physics Letters A*, vol. 140, no. 7, pp. 447–450, 1989.

[30] B. Kramer, J. Mašek, V. Špička, and B. Velický, “Coherent electronic transport properties of quasi-one-dimensional systems,” *Surface Science*, vol. 229, no. 1, pp. 316–320, 1990.

[31] J. Wróbel, F. Kuchar, K. Ismail, K. Lee, H. Nickel, and W. Schlapp, “Quantized conductance of a quasi-ballistic one-dimensional wire,” *Surface science*, vol. 263, no. 1, pp. 261–264, 1992.

[32] J. Wróbel, F. Kuchar, K. Ismail, K. Lee, H. Nickel, W. Schlapp, G. Grabecki, and T. Dietl, “The influence of reduced dimensionality on the spin-splitting in gaalas/gaas quantum wires,” *Surface science*, vol. 305, no. 1, pp. 615–619, 1994.

[33] S. Winnerl, M. Orlita, P. Plochocka, P. Kossacki, M. Potemski, T. Winzer, E. Malic, A. Knorr, M. Sprinkle, C. Berger *et al.*, “Carrier relaxation in epitaxial graphene photoexcited near the dirac point,” *Physical review letters*, vol. 107, no. 23, p. 237401, 2011.

[34] J. H. Strait, H. Wang, S. Shivaraman, V. Shields, M. Spencer, and F. Rana, “Very slow cooling dynamics of photoexcited carriers in graphene observed by optical-pump terahertz-probe spectroscopy,” *Nano letters*, vol. 11, no. 11, pp. 4902–4906, 2011.

[35] J. C. Johannsen, S. Ulstrup, F. Cilento, A. Crepaldi, M. Zacchigna, C. Cacho, I. E. Turcu, E. Springate, F. Fromm, C. Raidel *et al.*, “Direct view of hot carrier dynamics in graphene,” *Physical review letters*, vol. 111, no. 2, p. 027403, 2013.

[36] I. Gierz, J. C. Petersen, M. Mitrano, C. Cacho, I. E. Turcu, E. Springate, A. Stöhr, A. Köhler, U. Starke, and A. Cavalleri, “Snapshots of non-equilibrium dirac carrier distributions in graphene,” *Nature materials*, vol. 12, no. 12, pp. 1119–1124, 2013.

[37] P. A. George, J. Strait, J. Dawlaty, S. Shivaraman, M. Chandrashekhar, F. Rana, and M. G. Spencer, “Ultrafast optical-pump terahertz-probe spectroscopy of the carrier relaxation and recombination dynamics in epitaxial graphene,” *Nano letters*, vol. 8, no. 12, pp. 4248–4251, 2008.

[38] G. Jnawali, Y. Rao, H. Yan, and T. F. Heinz, “Observation of a transient decrease in terahertz conductivity of single-layer graphene induced by ultrafast optical excitation,” *Nano letters*, vol. 13, no. 2, pp. 524–530, 2013.

[39] Y. Yang and R. Murali, “Impact of size effect on graphene nanoribbon transport,” *Electron Device Letters, IEEE*, vol. 31, no. 3, pp. 237–239, 2010.

[40] A. D. Liao, J. Z. Wu, X. Wang, K. Tahy, D. Jena, H. Dai, and E. Pop, “Thermally limited current carrying ability of graphene nanoribbons,” *Physical review letters*, vol. 106, no. 25, p. 256801, 2011.

[41] S. Thongrattanasiri, A. Manjavacas, and F. J. García de Abajo, “Quantum finite-size effects in graphene plasmons,” *Acs Nano*, vol. 6, no. 2, pp. 1766–1775, 2012.

[42] P. Romanets and F. Vasko, “Transient response of intrinsic graphene under ultrafast interband excitation,” *Physical Review B*, vol. 81, no. 8, p. 085421, 2010.

[43] W.-K. Tse and S. D. Sarma, “Energy relaxation of hot dirac fermions in graphene,” *Physical Review B*, vol. 79, no. 23, p. 235406, 2009.

[44] D. Bischoff, A. Varlet, P. Simonet, M. Eich, H. Overweg, T. Ihn, and K. Ensslin, “Localized charge carriers in graphene nanodevices,” *Applied Physics Reviews*, vol. 2, no. 3, p. 031301, 2015.

[45] A. Kimouche, M. M. Ervasti, R. Drost, S. Halonen, A. Harju, P. M. Joensuu, J. Sainio, and P. Liljeroth, “Ultra-narrow metallic armchair graphene nanoribbons,” *Nature communications*, vol. 6, 2015.

[46] R. M. Jacobberger, B. Kiraly, M. Fortin-Deschenes, P. L. Levesque, K. M. McElhinny, G. J. Brady, R. R. Delgado, S. S. Roy, A. Mannix, M. G. Lagally *et al.*, “Direct oriented growth of armchair graphene nanoribbons on germanium,” *Nature communications*, vol. 6, 2015.

[47] H. Shen, Y. Shi, and X. Wang, “Synthesis, charge transport and device applications of graphene nanoribbons,” *Synthetic Metals*, vol. 210, pp. 109–122, 2015.

[48] E. Rotenberg, A. Bostwick, T. Ohta, J. L. McChesney, T. Seyller, and K. Horn, “Origin of the energy bandgap in epitaxial graphene,” *Nature materials*, vol. 7, no. 4, pp. 258–259, 2008.

[49] F. Xia, V. Perebeinos, Y.-m. Lin, Y. Wu, and P. Avouris, “The origins and limits of metal-graphene junction resistance,” *Nature nanotechnology*, vol. 6, no. 3, pp. 179–184, 2011.

[50] Y.-C. Chen, T. Cao, C. Chen, Z. Pedramrazi, D. Haberer, D. G. de Oteyza, F. R. Fischer, S. G. Louie, and M. F. Crommie, “Molecular bandgap engineering of bottom-up synthesized graphene nanoribbon heterojunctions,” *Nature nanotechnology*, vol. 10, no. 2, pp. 156–160, 2015.

[51] M. Born and E. Wolf, *Principles of Optics*, 7th ed. Cambridge, UK: Cambridge University Press, 1999.